

# A unified Pythagorean hodograph approach to the medial axis transform and offset approximation

Kosinka, Jiri; Lávicka, Miroslav

*Published in:*
Journal of Computational and Applied Mathematics

*DOI:*
10.1016/j.cam.2011.02.001



*Publication date:*
2011

Journal of Computational and Applied Mathematics 235 (2011) 3413–3424

Contents lists available at ScienceDirect

Journal of Computational and Applied Mathematics

journal homepage: www.elsevier.com/locate/cam

# A unified Pythagorean hodograph approach to the medial axis transform and offset approximation

Jiří Kosinka, Miroslav Lávička *

*University of West Bohemia, Faculty of Applied Sciences, Department of Mathematics, Univerzitní 8, 301 00 Plzeň, Czech Republic*

ARTICLE INFO

*Article history:*
Received 23 August 2010
Received in revised form 24 November 2010

*Keywords:*
Pythagorean hodograph curve
Medial axis transform
Minkowski space
Hermite interpolation
Trimmed offsets

ABSTRACT

Algorithms based on Pythagorean hodographs (PH) in the Euclidean plane and in Minkowski space share common goals, the main one being rationality of offsets of planar domains. However, only separate interpolation techniques based on these curves can be found in the literature. It was recently revealed that rational PH curves in the Euclidean plane and in Minkowski space are very closely related. In this paper, we continue the discussion of the interplay between spatial MPH curves and their associated planar PH curves from the point of view of Hermite interpolation. On the basis of this approach we design a new, simple interpolation algorithm. The main advantage of the unifying method presented lies in the fact that it uses, after only some simple additional computations, an arbitrary algorithm for interpolation using planar PH curves also for interpolation using spatial MPH curves. We present the functionality of our method for $G^1$ Hermite data; however, one could also obtain higher order algorithms.



## 1. Introduction

Curve and surface offsets are geometric objects that are frequently used in various technical applications, e.g. numerically controlled machining and computer-aided manufacturing. Due to their wide applicability, studying classical (and also general) offsets of hypersurfaces has recently become an active and popular research area. Many interesting problems related to this topic have arisen, including those of the analysis of geometric and algebraic properties of offsets, determining the number and type of offset components and constructing rational parametrisations of offsets; cf. [1–7].

Describing a tool path in NURBS form is currently a universal standard in technical applications. However, free-form NURBS do not possess rational offsets in general and thus techniques of approximation for offsets must be used, especially in connection with CAD/CAM systems. Since offset approximation and trimming is usually performed at the expense of great computational effort, it is worthwhile to investigate suitable exact techniques and to study curves and surfaces with exact rational offsets. This approach led to the definition of Pythagorean hodograph (PH) curves in [8]. These special curves can be used for formulating efficient approximation and interpolation techniques for free-form shapes. Comparing methods based on PH curves to the classical approximation, not the offset but the base curve is approximated. This guarantees that all corresponding offset curves are rational and mutually equidistant, and only one approximation step is required even if more than one offset is needed.

Later, the concept of polynomial planar PH curves was generalized to space PH curves [9–13], to rational PH curves [14,15] and to the so called Pythagorean normal vector (PN) surfaces [14,1,16,17]. For a survey of shapes with Pythagorean normals (i.e., possessing rational offsets), see [18]. However, even though these shapes admit rational offsets, the usually most

* Corresponding author.
*E-mail addresses:* kosinka@kma.zcu.cz (J. Kosinka), lavicka@kma.zcu.cz (M. Lávička).

0377-0427/$ – see front matter © 2011 Elsevier B.V. All rights reserved.
doi:10.1016/j.cam.2011.02.001

demanding part of the construction process is trimming. In practice, not the whole offset but only some of its parts are used.

As observed in [19], using the medial axis transform (MAT) representation makes the trimming procedure of inner offsets considerably simpler – only those parts of the MAT where the corresponding circle radius is less than the offset distance have to be trimmed. This gives a strong justification for studying approximation and interpolation techniques based on the so called Minkowski Pythagorean hodograph (MPH) curves. Polynomial MPH curves were defined in [20] and later generalized to rational MPH curves in [21]. Indeed, if a part of the medial axis transform of a planar domain is an MPH curve, then the corresponding domain boundary segments and all their offsets possess rational parametrisations. Interpolation and approximation methods based on MPH curves were thoroughly investigated in e.g. [22–27].

Although algorithms based on Pythagorean hodographs in the Euclidean plane and in Minkowski space share common goals, the main one being rationality of offsets of planar domains, there exist many efficient but separate techniques for Hermite interpolation based on PH and MPH curves. This shortcoming motivates the search for a unifying computational approach. The main advantage of the method presented in this paper lies in the fact that it directly uses, after only some simple completing operations, an arbitrary algorithm for interpolation using planar PH curves also for interpolation using spatial MPH curves. All details of our approach are discussed in the following sections. At this point we only reveal that this technique is based on the close interplay between spatial MPH curves and associated planar PH curves studied in [21].

The remainder of this paper is organized as follows. Section 2 recalls some basic facts concerning Euclidean and Minkowski Pythagorean hodograph curves, medial axis transforms and envelopes of one-parameter families of circles. Section 3 is devoted to a novel interpolation method with MPH curves based on planar PH splines. In this section, we formulate and analyse an algorithm for $G^1$ Hermite interpolation via MPH curves. The algorithm is then demonstrated on several examples in Section 4. Finally, we conclude the paper in Section 5.

## 2. Preliminaries

We briefly review fundamentals of rational curves with Pythagorean hodographs in the Euclidean plane and in Minkowski space and recall their close interplay. The reader is referred to [18,21] for more details.

### 2.1. Rational curves with rational offsets in the Euclidean plane

Consider a $C^1$ parametric curve $\mathbf{x}(t) = (x_1(t), x_2(t))^\top$. The *δ-offset* of $\mathbf{x}(t)$ is the set of all points in $\mathbb{R}^2$ that lie at a distance $\delta$ from $\mathbf{x}(t)$. The two branches of the offset are given by

$$\mathbf{x}_\delta(t) = \mathbf{x}(t) \pm \delta\mathbf{n}(t), \qquad \mathbf{n}(t) = \frac{\mathbf{x}'(t)^\perp}{\|\mathbf{x}'(t)\|}, \tag{1}$$

where $\|\cdot\|$ denotes the usual Euclidean norm and $\mathbf{x}'(t)^\perp = (x_2'(t), -x_1'(t))^\top$ is the rotation of $\mathbf{x}'(t)$ about the origin by the angle $-\frac{\pi}{2}$.

A study of offset rationality led to the class of planar *Pythagorean hodograph* (PH) curves (i.e., curves with rational offsets) introduced in [8]. Rational PH curves are defined as rational curves $\mathbf{x}(t) = (x_1(t), x_2(t))^\top$ fulfilling the (Euclidean) *PH condition*

$$\mathbf{x}'(t) \cdot \mathbf{x}'(t) = x_1'(t)^2 + x_2'(t)^2 = \sigma(t)^2, \tag{2}$$

where $\sigma(t) \in \mathbb{R}(t)$ is a rational function and '$\cdot$' denotes the standard Euclidean inner product. In order to avoid working with piecewise representations, we consider only curves for which $\sigma(t) > 0$ in the interval of interest for the remainder of the paper. Then, $\sigma(t)$ will be called the *speed* of $\mathbf{x}(t)$.

A parametric representation of all planar rational PH curves can be obtained from their dual representation

$$(2kl : k^2 - l^2 : -g) \tag{3}$$

in the form (cf. [14,15])

$$x_1 = \frac{2(ll' - kk')g + (k^2 - l^2)g'}{2(k^2 + l^2)(kl' - k'l)}, \qquad x_2 = \frac{(k'l + kl')g - klg'}{(k^2 + l^2)(kl' - k'l)}, \tag{4}$$

where $k(t)$, $l(t)$ are relatively prime polynomials and $g(t) = e(t)/f(t)$ is a rational function.

Pythagorean hodograph curves were originally introduced in [8] as *planar polynomial* curves. These can be readily obtained from the general formula (4) by setting

$$e(t) = 2kl \int (k^2 - l^2)m \,\mathrm{d}t - (k^2 - l^2) \int 2klm \,\mathrm{d}t, \qquad f(t) = \text{constant}, \tag{5}$$

where $m(t)$ is an arbitrary polynomial; see [15]. Consequently, we arrive at

$$x_1' = m(k^2 - l^2), \qquad x_2' = 2mkl, \qquad \sigma = m(k^2 + l^2), \tag{6}$$

which describes all polynomial solutions of (2), i.e., all polynomial PH curves in $\mathbb{R}^2$.

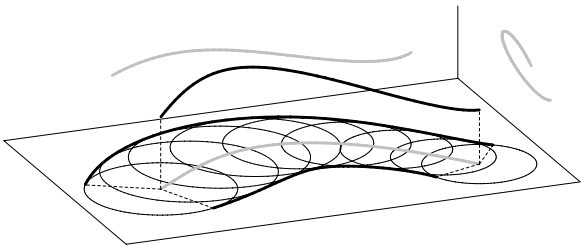

**Fig. 1.** A domain $\Omega$ and its maximal inscribed discs, MA($\Omega$) and MAT($\Omega$).

### 2.2. Curves with Pythagorean hodographs in Minkowski space

Consider a planar domain $\Omega \subset \mathbb{R}^2$ and the family of all inscribed discs in $\Omega$ partially ordered with respect to inclusion; see Fig. 1. An inscribed disc is called maximal if it is not contained in any other inscribed disc. Then the *medial axis* MA($\Omega$) is the locus of all centres $(y_1, y_2)^\top$ of maximal inscribed discs and the *medial axis transform* MAT($\Omega$) is obtained by appending the corresponding disc radii $y_3$ to the medial axis, i.e., MAT consists of points $\mathbf{y} = (y_1, y_2, y_3)^\top$. The projection

$$\mathbb{R}^{2,1} \to \mathbb{R}^2 : \mathbf{y} = (y_1, y_2, y_3)^\top \mapsto \overset{\triangledown}{\mathbf{y}} = (y_1, y_2)^\top \tag{7}$$

naturally relates MA to MAT (read $\overset{\triangledown}{\mathbf{y}}$ as '$\mathbf{y}$ down'). The notion of MAT can also be extended to other shapes. For example for two curve segments (see Fig. 1), we replace maximal discs with discs touching both segments. We will use the notions of MA and MAT in this more general sense. Moreover, in order to avoid a discussion on topology, we consider only segments of MAT whose points correspond to maximal circles having precisely two contact points. For a complete treatment of the MAT topology the reader is referred to [28,19].

For a $C^1$ segment $\mathbf{y}(t) = (y_1(t), y_2(t), y_3(t))^\top$ of MAT($\Omega$) we can compute the corresponding boundary of $\Omega$ from the envelope formula (cf. [19,20]) in the form

$$\mathbf{x}_\pm(t) = \begin{pmatrix} y_1 \\ y_2 \end{pmatrix} - \frac{y_3}{{y_1'}^2 + {y_2'}^2} \left[ y_3' \begin{pmatrix} y_1' \\ y_2' \end{pmatrix} \pm \sqrt{{y_1'}^2 + {y_2'}^2 - {y_3'}^2} \begin{pmatrix} -y_2' \\ y_1' \end{pmatrix} \right]. \tag{8}$$

A study of rationality of envelopes (8) led to the class of *Minkowski Pythagorean hodograph* (MPH) curves introduced in [20]. MPH curves are defined as rational curves $\mathbf{y}(t) = (y_1(t), y_2(t), y_3(t))^\top$ in three-dimensional space fulfilling the condition

$${y_1'}^2(t) + {y_2'}^2(t) - {y_3'}^2(t) = \varrho^2(t), \tag{9}$$

where $\varrho(t) \in \mathbb{R}(t)$. The PH condition (2) is now fulfilled with respect to the indefinite *Minkowski inner product*

$$\langle \mathbf{u}, \mathbf{v} \rangle = u_1 v_1 + u_2 v_2 - u_3 v_3, \tag{10}$$

which makes *Minkowski space* $\mathbb{R}^{2,1}$ the natural ambient space for MPH curves. Again, as in the case of PH curves, we, without loss of generality, restrict ourselves to $\varrho(t) > 0$ only. Then, $\varrho(t)$ will be called the *Minkowski speed* of $\mathbf{y}(t)$.

The *squared norm* of a vector $\mathbf{u} \in \mathbb{R}^{2,1}$, defined by $\langle \mathbf{u}, \mathbf{u} \rangle$, can be positive, negative or zero. Hence, we distinguish three kinds of vectors: *space-like* if $\langle \mathbf{u}, \mathbf{u} \rangle > 0$, *time-like* if $\langle \mathbf{u}, \mathbf{u} \rangle < 0$, and *light-like* (or *isotropic*) if $\langle \mathbf{u}, \mathbf{u} \rangle = 0$. Due to the form of (9), the tangent vector $\mathbf{y}'(t)$ of an MPH curve can be space-like or light-like only.

As discussed in [19,20], if MAT($\Omega$) is an MPH curve $\mathbf{y}$, then the boundary curves $\mathbf{x}_\pm$ of $\Omega$ associated with $\mathbf{y}$ and all offsets of the boundary are (piecewise) rational; cf. (8). We rewrite (8) in the form

$$\mathbf{x}_\pm = \overset{\triangledown}{\mathbf{y}} - y_3 \mathbf{n}_\pm, \tag{11}$$

where

$$\mathbf{n}_\pm = \frac{1}{\varrho^2 + y_3'^2} \begin{pmatrix} y_3' y_1' \mp \varrho y_2' \\ y_3' y_2' \pm \varrho y_1' \end{pmatrix} = \frac{1}{\varrho^2 + y_3'^2} (y_3' \overset{\triangledown}{\mathbf{y}}' \mp \varrho \overset{\triangledown'^{\perp}}{\mathbf{y}}). \tag{12}$$

It can be shown by a direct computation that $\mathbf{n}_\pm$ is a unit vector perpendicular to $\mathbf{x}_\pm$. Moreover, $\mathbf{n}_\pm$ is rational if and only if $\varrho$ is rational. Hence, for any MPH curve $\mathbf{y} \subset \mathbb{R}^{2,1}$, the *associated* curves $\mathbf{x}_\pm \subset \mathbb{R}^2$ possess a normal vector field rationally parametrising the unit circle, i.e., $\mathbf{x}_\pm$ are rational PH curves.

This observation is closely related to the result of [21], which states that any rational MPH curve $\mathbf{y}$ in $\mathbb{R}^{2,1}$ can be constructed starting from an (associated) planar rational PH curve $\mathbf{x}$ in $\mathbb{R}^2$ and a rational function $r$ in the form

$$\mathbf{y}(t) = (x_1 + r n_1, x_2 + r n_2, r)^\top = \overset{\triangle}{\mathbf{x}}(t) + r(t) \tilde{\mathbf{n}}(t), \tag{13}$$

with $\overset{\triangle}{\mathbf{x}} = (x_1, x_2, 0)^\top$ (read $\overset{\triangle}{\mathbf{x}}$ as '$\mathbf{x}$ up') and $\tilde{\mathbf{n}} = (n_1, n_2, 1)^\top$, where $\mathbf{n} = (n_1, n_2)^\top = \mathbf{x}'^{\perp}/\sigma$. We remark that $\mathbf{x}$ will play the role of $\mathbf{x}_+$ in what follows. Substituting (4) into (13), one can obtain an expression for all rational MPH curves; see formula (30) in [21].

Analogously to the planar Euclidean case, polynomial MPH curves form a proper subset of the rational ones and are given by

$$y_1' = km - ln, \qquad y_2' = -kn - lm, \qquad y_3' = -kn + lm, \qquad \varrho = km + ln. \tag{14}$$

This is an alternative to the original formula for polynomial MPH curves presented in [20].

### 2.3. Validity and a local canonical form of medial axis transforms

When working with the medial axis transform as a shape representation, one has to guarantee that the associated domain boundary obtained by the envelope formula (8) is a valid boundary. Consider a $C^1$ curve $\mathbf{y} \in \mathbb{R}^{2,1}$. This curve is the MAT of some planar domain only if the following constraints are satisfied.

The boundary curves $\mathbf{x}_\pm$ (cf. (8)) are real provided that

$$\langle \mathbf{y}', \mathbf{y}' \rangle \geq 0, \tag{15}$$

which becomes the first constraint on $\mathbf{y}$. In other words, the tangent vector of $\mathbf{y}$ must not be time-like.

In order to eliminate singularities and also points with reversed boundary orientation, we require that

$$\mathbf{x}' \cdot \overset{\triangledown}{\mathbf{y}}{}' > 0. \tag{16}$$

A direct computation shows that (16) is equivalent to

$$1 + y_3 \kappa > 0, \tag{17}$$

where $\kappa(t) = (x_1' x_2'' - x_1'' x_2')/\sigma^3$ is the signed Euclidean curvature of $\mathbf{x}(t)$. This condition is automatically satisfied for points with non-negative curvature. On the other hand, at points where $\kappa < 0$, (17) is equivalent to $y_3 < \rho$, where $\rho$ is the radius of the osculating circle of $\mathbf{x}$. This natural condition becomes the second validity constraint.

Consequently, a curve $\mathbf{y} \in \mathbb{R}^{2,1}$ considered as an MAT will be called a *valid* MAT provided that it satisfies constraints (15) and (17). More details about the validity of MATs can be found e.g. in [29–31]. We will use the above constraints in Section 3, where an algorithm for Hermite interpolation with MPH curves using associated PH curves is designed and analysed.

For future use we recall some basic facts from differential geometry of curves in $\mathbb{R}^{2,1}$. Let $\mathbf{y}(s) = (y_1(s), y_2(s), y_3(s))^\top$ be a sufficiently smooth space-like curve with no Minkowski inflections parametrised by the arc length and let $\mathbf{T} = \mathbf{y}'(s)$ be its unit (space-like) tangent vector, i.e., $\langle \mathbf{T}, \mathbf{T} \rangle = 1$ and $\langle \mathbf{T}', \mathbf{T}' \rangle \neq 0$. The curve $\mathbf{y}(s)$ can be considered as a (valid) MAT of a planar domain. Then the Frenet formulae take the form

$$\begin{aligned} \mathbf{T}' &= \varkappa \mathbf{N}, \\ \mathbf{N}' &= -\langle \mathbf{N}, \mathbf{N} \rangle \varkappa \mathbf{T} + \tau \mathbf{B}, \\ \mathbf{B}' &= \tau \mathbf{N}. \end{aligned} \tag{18}$$

The vectors $\mathbf{N}$ and $\mathbf{B}$ are the unit *normal* and *binormal* vectors, respectively, and $\varkappa > 0$ and $\tau$ are the *Minkowski curvature* and *torsion* of $\mathbf{y}(s)$. Using (18) allows us to compute the derivatives of $\mathbf{y}(s)$ at $s = 0$ as

$$\begin{aligned} \mathbf{y}'(0) &= \mathbf{T}_0, \\ \mathbf{y}''(0) &= \mathbf{T}'(0) = \varkappa_0 \mathbf{N}_0, \\ \mathbf{y}'''(0) &= \varkappa_1 \mathbf{N}_0 + \varkappa_0 \mathbf{N}'(0) = \varkappa_1 \mathbf{N}_0 \mp (\varkappa_0^2 \mathbf{T}_0 + \varkappa_0 \tau_0 \mathbf{B}_0), \end{aligned} \tag{19}$$

etc., where $\mathbf{T}_0 = \mathbf{T}(0)$, $\mathbf{N}_0 = \mathbf{N}(0)$, $\mathbf{B}_0 = \mathbf{B}(0)$, $\varkappa_0 = \varkappa(0)$, $\varkappa_1 = \varkappa'(0)$, $\tau_0 = \tau(0)$, etc. The choice of the sign in $\mathbf{y}'''(0)$ (and all further derivatives) depends on $\langle \mathbf{N}_0, \mathbf{N}_0 \rangle$ (cf. (18)), i.e., the type of the normal vector $\mathbf{N}_0$. Finally, with the help of (19) we generate the *local canonical form* of $\mathbf{y}(s)$

$$\mathbf{y}(s) = \mathbf{y}(0) + s\mathbf{y}'(0) + \frac{s^2}{2}\mathbf{y}''(0) + \frac{s^3}{6}\mathbf{y}'''(0) + \cdots. \tag{20}$$

More details, especially on Minkowski inflections, can be found in [24].

### 2.4. Polynomial domain boundaries and the isotropic surface

Let us now study the relation between rational domain boundaries associated with an MPH curve describing the medial axis transform of a planar domain. Since the points $\mathbf{x}_+$ and $\mathbf{x}_-$ are symmetric along the tangent of the medial axis $\overset{\triangledown}{\mathbf{y}}$ (see Fig. 3), we obtain that

$$\mathbf{x}_- = \mathbf{x}_+ - 2\frac{\overset{\triangledown}{\mathbf{y}}{}'^{\perp} \cdot (\mathbf{x}_+ - \overset{\triangledown}{\mathbf{y}})}{y_1'^2 + y_2'^2} \overset{\triangledown}{\mathbf{y}}{}'^{\perp}. \tag{21}$$

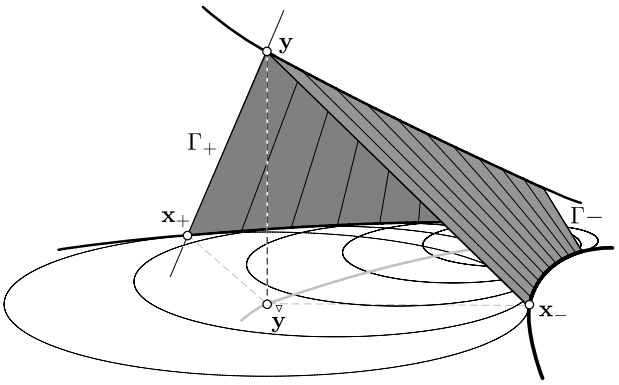


**Fig. 2.** Isotropic surface $\Gamma_{\pm} \subset \mathbb{R}^{2,1}$ corresponding to $\mathbf{x}_{\pm} \subset \mathbb{R}^2$ and $\mathbf{y} \subset \mathbb{R}^{2,1}$.

In particular, for a polynomial MPH curve given by (14) we arrive at the special envelope formula (cf. (8))

$$\mathbf{x}_+ = \overset{\triangledown}{\mathbf{y}} + \frac{y_3}{k^2+l^2}\begin{pmatrix} 2kl \\ k^2-l^2 \end{pmatrix}, \qquad \mathbf{x}_- = \overset{\triangledown}{\mathbf{y}} - \frac{y_3}{m^2+n^2}\begin{pmatrix} 2mn \\ m^2-n^2 \end{pmatrix}. \tag{22}$$

Now, let $\mathbf{y}$ be polynomial. The above relations show that both $\mathbf{x}_+$ and $\mathbf{x}_-$ are still rational. Also, if e.g. $\mathbf{x}_+$ is polynomial, then $\mathbf{x}_-$ is in general rational. Therefore, the most prominent role is played by polynomial MPH curves given by a polynomial (associated) PH curve $\mathbf{x}(t) \subset \mathbb{R}^2$ and a polynomial $r(t)$. Recalling (6) and (13), the term $\sigma(t)$ has to divide the polynomial $r(t)$ in this case, i.e., there exists a polynomial $p(t)$ such that $r(t) = p(t)\sigma(t)$. Summing up, we obtain

$$\mathbf{y}(t) = (x_1(t) + p(t)x_2'(t), x_2(t) - p(t)x_1'(t), p(t)\sigma(t))^{\top}. \tag{23}$$

Finally, let $\mathbf{x}(t)$ be a polynomial PH curve of degree $d_1$ and $r(t)$ be a polynomial of degree $d_2$. Then the rational degree of $\mathbf{y}(t)$ amounts to at most $[d_1 - 1 + \max(d_1, d_2), d_1 - 1]$. In particular, for (23) we obtain

$$\deg(\mathbf{y}) = d_1 + d_3 - 1, \tag{24}$$

where $d_3$ is the degree of $p(t)$.

For later use we recall the notion of isotropic surfaces. Starting from a curve $\mathbf{x}(t) \subset \mathbb{R}^2$, the corresponding *isotropic surface* $\Gamma \subset \mathbb{R}^{2,1}$ [32–34] is given by the equation

$$\Gamma : \mathbf{y}(t, s) = \overset{\triangle}{\mathbf{x}}(t) + s\tilde{\mathbf{n}}(t). \tag{25}$$

It holds that

$$\langle \mathbf{y}(t,s) - \overset{\triangle}{\mathbf{x}}, \mathbf{y}(t,s) - \overset{\triangle}{\mathbf{x}} \rangle = s^2 \langle \tilde{\mathbf{n}}, \tilde{\mathbf{n}} \rangle = s^2(\|\mathbf{n}\|^2 - 1) = 0, \tag{26}$$

and thus $\Gamma$ is a ruled (and in fact developable) surface consisting of straight lines through $\mathbf{x}$ given by light-like vectors $\mathbf{y}(t,s) - \overset{\triangle}{\mathbf{x}}(t)$.

Next, if $\mathbf{x}(t)$ is a PH curve, $\Gamma$ is a (piecewise) rational surface. Hence, all MPH curves $\mathbf{y}(t)$ given by (13) are rational curves on the rational surface (25) obtained by setting $s = r(t) \in \mathbb{R}(t)$. Starting from PH curves $\mathbf{x}_+(t)$ and $\mathbf{x}_-(t)$, the corresponding isotropic surfaces $\Gamma_+$ and $\Gamma_-$ intersect in the associated MPH curve $\mathbf{y}(t)$; cf. Fig. 2. Clearly, planar sections of $\Gamma_{\pm}$ parallel to $\mathbb{R}^2$ lead to $\delta$-offsets of the associated domain boundaries.

## 3. Hermite interpolation using MPH curves using associated PH curves

The two-point geometric Hermite interpolation problem consists in finding a curve that passes through two given points and matches (unit) tangent vectors at these points. Motivated by (23), we introduce a straightforward and very simple algorithm for $G^1$ Hermite MPH interpolation of given data $\mathcal{D} = \{\mathbf{y}_0, \mathbf{y}_1; \mathbf{t}_0, \mathbf{t}_1\}$.

More precisely, a polynomial MPH curve $\mathbf{y}(t)$ is to interpolate the end points

$$\mathbf{y}(i) = \mathbf{y}_i = (y_{i1}, y_{i2}, y_{i3})^{\top}, \quad i \in \{0, 1\}, \tag{27}$$

which satisfy that $\mathbf{y}_1 - \mathbf{y}_0$ is not time-like, and the end tangent vectors

$$\mathbf{y}'(i) = \lambda_i \mathbf{t}_i = \lambda_i (t_{i1}, t_{i2}, t_{i3})^{\top}, \quad i \in \{0, 1\}. \tag{28}$$

Using the results from Section 2.4, we need to find a polynomial PH curve $\mathbf{x}(t)$ and a polynomial $p(t)$ such that (23) fulfils the interpolation conditions, i.e., $\mathbf{y}(t)$ is required to match $\mathcal{D} = \{\mathbf{y}_0, \mathbf{y}_1; \mathbf{t}_0, \mathbf{t}_1\}$. A detailed description of the particular steps of our interpolation technique follows.

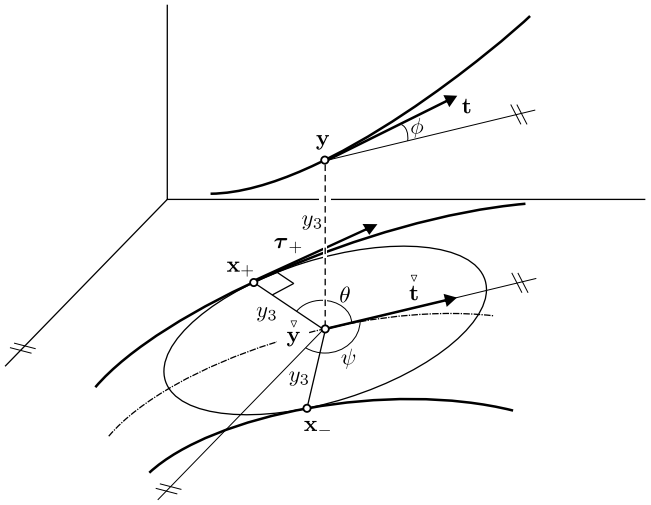


**Fig. 3.** Spatial/planar $G^1$ Hermite data for interpolation using MPH/PH curves (note that $\phi$ is a hyperbolic angle).

### 3.1. Step 1: Mapping given spatial data to the plane

The fundamental relation between $\Omega$ and MAT($\Omega$) consists in the fact that each contact disc of $\Omega$ corresponds to a point in $\mathbb{R}^{2,1}$. Nevertheless, we can easily obtain higher order relations.

Consider a point $\mathbf{y}$ on a curve in $\mathbb{R}^{2,1}$ with the associated space-like unit tangent vector (with respect to the Minkowski metric)

$$\mathbf{t} = (\cos\psi\cosh\phi, \sin\psi\cosh\phi, \sinh\phi)^{\top}, \quad \text{where } \phi \in \mathbb{R},\ \psi \in [0, 2\pi). \tag{29}$$

We take the corresponding contact disc centred at $\overset{\triangledown}{\mathbf{y}}(t) = (y_1, y_2)^{\top} \in \mathbb{R}^2$ with radius $y_3$ and the associated contact points $\mathbf{x}_+$ and $\mathbf{x}_-$. The orthogonal projection $\overset{\triangledown}{\mathbf{t}} = (\cos\psi\cosh\phi, \sin\psi\cosh\phi)^{\top}$ of the tangent vector $\mathbf{t}$ bisects the angle $\angle(\mathbf{x}_- \overset{\triangledown}{\mathbf{y}} \mathbf{x}_+)$ in the direction of the domain. We denote the half-angle obtained by $\theta \in (0, \pi)$; see Fig. 3.

It can be checked that $-\cos\theta$ is the rate at which the radius increases and thus the curve representing an MAT in $\mathbb{R}^{2,1}$ has the slope

$$\tanh\phi = -\cos\theta \tag{30}$$

at the point $\mathbf{y}$; cf. [28,19] for more details. Next, defining

$$\alpha_+ = \psi + \theta, \qquad \alpha_- = \psi - \theta \tag{31}$$

we arrive at the expressions for contact points

$$\mathbf{x}_+ = \overset{\triangledown}{\mathbf{y}} + y_3(\cos\alpha_+, \sin\alpha_+)^{\top}, \qquad \mathbf{x}_- = \overset{\triangledown}{\mathbf{y}} + y_3(\cos\alpha_-, \sin\alpha_-)^{\top}; \tag{32}$$

cf. (11) for general MATs and (22) for polynomial MPH curves. The associated unit tangent vectors of the boundary of $\Omega$ at the contact points $\mathbf{x}_+, \mathbf{x}_-$ are

$$\boldsymbol{\tau}_+ = (\sin\alpha_+, -\cos\alpha_+)^{\top}, \qquad \boldsymbol{\tau}_- = (-\sin\alpha_-, \cos\alpha_-)^{\top}. \tag{33}$$

To sum up, formulae (32) and (33) show how to obtain the $G^1$ planar data $\overline{\mathcal{D}} = \{\mathbf{x}_0, \mathbf{x}_1; \boldsymbol{\tau}_0, \boldsymbol{\tau}_1\}$ from $\mathcal{D}$ for polynomial PH interpolation.

Since not all curves describe a feasible MAT (see Section 2.3), we have to study the validity condition (16) with respect to the given and transformed data $\mathcal{D}$ and $\overline{\mathcal{D}}$. For $\boldsymbol{\tau}_+$ (which plays the role of $\boldsymbol{\tau}$ in what follows) we arrive at

$$\boldsymbol{\tau}_+ \cdot \overset{\triangledown}{\mathbf{t}} = \cosh\phi\sin\theta = \cosh\phi\sqrt{1-\tanh^2\phi} = \cosh\phi\frac{1}{\cosh\phi} = 1 > 0, \tag{34}$$

i.e., the condition is generally satisfied for all situations considered.

Finally, we summarize some important expressions relating the above introduced quantities. It holds that

$$\langle\tilde{\mathbf{n}}, \tilde{\mathbf{n}}\rangle = 0, \qquad \langle\tilde{\mathbf{n}}, \mathbf{t}\rangle = 0, \qquad \langle\tilde{\mathbf{n}}, \overset{\triangle}{\boldsymbol{\tau}}\rangle = 0, \tag{35}$$

where $\tilde{\mathbf{n}} = (n_1, n_2, 1)^{\top}$ is the direction vector of an isotropic line on the surface $\Gamma(t, s)$. These relations can be easily derived from the properties of the isotropic surface $\Gamma(t, s)$; cf. Section 2.4. The vector $\tilde{\mathbf{n}}$ can be identified with (normalized) $\mathbf{y} - \overset{\triangle}{\mathbf{x}}$ provided that it does not vanish.

### 3.2. Step 2: Hermite interpolation using a planar PH curve

Without loss of generality we may choose only one branch of the envelope corresponding to the MPH curve $\mathbf{y}(t)$. We consider $\mathbf{x}(t) = \mathbf{x}_+(t)$ as mentioned earlier. Following Step 1, $\mathbf{x}(t)$, a planar polynomial PH curve, is to interpolate $\overline{\mathcal{D}}$.

Our algorithm is independent from a particular procedure for Hermite interpolation using planar PH curves. Obviously, this step can be easily replaced by a better or new technique. Nevertheless, we need some well-known testing procedure to present the functionality of our method.

For the sake of illustration, we have chosen a variant [35] of the algorithm introduced in [36], which uses simple (i.e., not self-intersecting) arcs of the *Tschirnhausen cubic* as interpolants. The Tschirnhausen cubic is the simplest non-trivial example of a planar polynomial PH curve with the standard parametrisation $\mathbf{x}(t) = (t^3/3 - t, t^2)^\top$ obtained by setting $k = t, l = 1, m = 1$ in (6). The reader interested in interpolation techniques using the Tschirnhausen cubic can find more details in [24,37,38]. The advantage is the low degree of the interpolating PH curve and hence also of the corresponding MPH interpolant.

We also remark that if the cubic PH interpolant for $\overline{\mathcal{D}}$ does not exist, we have two options. First, we can subdivide the spatial curve that the data $\mathcal{D}$ were originally sampled from. The results of Section 4 then guarantee that after a few steps of subdivision we can always match a cubic PH arc to the associated planar data. Second, we match the data $\mathcal{D}$ with a PH quintic. Even though this raises the degree of the resulting MPH interpolant, it also shows the flexibility of our method.

### 3.3. Step 3: From a PH to an MPH interpolant

Now, having the polynomial PH curve $\mathbf{x}(t)$ interpolating $\overline{\mathcal{D}}$ at hand (e.g. an arc of the Tschirnhausen cubic), we turn our attention to finding a suitable polynomial $p(t)$ such that $\mathbf{y}(t)$ interpolates the given spatial data. Recalling (23), we obtain

$$\mathbf{y}(t) = (x_1 + px_2', x_2 - px_1', p\sigma)^\top, \tag{36}$$

$$\mathbf{y}'(t) = (x_1' + p'x_2' + px_2'', x_2' - p'x_1' - px_1'', p'\sigma + p\sigma')^\top. \tag{37}$$

From (36), we immediately get

$$p_i = p(i) = \frac{y_{i3}}{\sigma(i)}, \quad i \in \{0, 1\}. \tag{38}$$

Defining $p_i' = p'(i)$, (37) gives the following interpolation conditions:

$$\begin{aligned} x_1'(i) + p_i'x_2'(i) + p_ix_2''(i) &= \lambda_i t_{i1}, \\ x_2'(i) - p_i'x_1'(i) - p_ix_1''(i) &= \lambda_i t_{i2}, \\ p_i'\sigma(i) + p_i\sigma'(i) &= \lambda_i t_{i3}. \end{aligned} \tag{39}$$

We have a system of three linear equations for two unknowns $p_i'$ and $\lambda_i$. However, considering $\langle \tilde{\mathbf{n}}, \mathbf{t} \rangle = 0$ (cf. (35)), we arrive at the following dependency condition:

$$n_1(x_1' + p'x_2' + px_2'') + n_2(x_2' - p'x_1' - px_1'') - (p'\sigma + p\sigma') = 0, \tag{40}$$

i.e., it is enough to consider only two equations in (39). For the sake of symmetry, we take the first two. This system of two linear equations for $\lambda_i$ and $p_i'$ can be solved using Cramer's rule. For $\lambda_i$ we obtain

$$\lambda_i = \sigma(i)(1 + y_{i3})\kappa(i), \tag{41}$$

since the determinant of the system is

$$\sigma(i)(\boldsymbol{\tau}_i \cdot \overset{\triangledown}{\mathbf{t}}(i)) = \sigma(i); \tag{42}$$

cf. (34). Now, taking into account the validity constraint (17) (cf. Section 2.3), we have guaranteed $\lambda_i > 0$ and thus the orientation of $\mathcal{D}$ is preserved. It only remains to compute

$$p_i' = \overset{\triangledown}{\mathbf{t}}(i) \cdot (p_i\mathbf{x}''(i) - \mathbf{x}'^{\perp}(i)). \tag{43}$$

Finally the polynomial $p(t)$ is determined by $p_0, p_1, p_0', p_1'$ and thus we can take $p(t)$ e.g. as the Ferguson cubic in the form

$$p(t) = (2t^3 - 3t^2 + 1)p_0 + (-2t^3 + 3t^2)p_1 + (t^3 - 2t^2 + t)p_0' + (t^3 - t^2)p_1'. \tag{44}$$

For a Tschirnhausen cubic interpolant and $p(t)$ being of degree 3, the resulting interpolating MPH curve $\mathbf{y}(t)$ is a quintic; see (24).

### 3.4. Summary

In this subsection, we summarize the main steps of the algorithm for computing an MPH curve matching given $G^1$ Hermite data $\mathcal{D}$:

**Algorithm 1** Compute an MPH interpolant for the given $G^1$ Hermite data

INPUT: Spatial $G^1$ Hermite data $\mathcal{D} = \{\mathbf{y}_0, \mathbf{y}_1; \mathbf{t}_0, \mathbf{t}_1\}$.

1. Compute the $G^1$ planar data $\overline{\mathcal{D}} = \{\mathbf{x}_0, \mathbf{x}_1; \boldsymbol{\tau}_0, \boldsymbol{\tau}_1\}$ corresponding to $\mathcal{D}$ by using formulae (32) and (33).
2. Interpolate among $\overline{\mathcal{D}}$ with a planar polynomial PH curve $\mathbf{x}(t)$ of degree $d_1$ using a suitable interpolation algorithm; see e.g. the references in Section 3.2.
3. Find a polynomial $p(t)$ of degree $d_3$ such that $\mathbf{y}(t)$ given by (23) interpolates among $\mathcal{D}$ (e.g. using (44)).

OUTPUT: A polynomial MPH curve $\mathbf{y}(t)$ of degree $d_1 + d_3 - 1$ matching the given data $\mathcal{D}$.

The main advantage of the algorithm presented, compared to other methods [24–26], is its simplicity and flexibility. An arbitrary technique for interpolation using planar PH curves can be used with only a few additional simple computations also for interpolation using spatial MPH curves. Our method is also suitable for computing approximations of domain boundaries and their trimmed offsets. This fact is shown in Section 5. Furthermore, our algorithm has another useful advantage—not only the MAT but also one of the boundary curves can be constructed as a polynomial curve.

All basic ideas of the algorithm are applicable also for interpolation using spatial *rational* MPH curves based on interpolation techniques using planar *rational* PH curves. On the other hand, rational PH techniques have not been sufficiently developed yet and one can find only a few $G^1$ Hermite interpolation algorithms based on rational PH curves; see e.g. [39–42]. Nonetheless, when a new efficient rational PH interpolation method is developed, the steps of Algorithm 1 can be simply adapted to accommodate the rational case as well.

## 4. Asymptotic analysis

In this section we study the asymptotic behaviour of the algorithm designed above. We apply, with slight modifications, the approach used in [24], where the existence and behaviour of interpolants for given regular and singular asymptotic data (i.e., when $\mathbf{N}_0$ is light-like) were thoroughly analysed. For the sake of brevity, we provide asymptotic analysis and results for regular data only and omit most of its technical parts. The interested reader is referred to the results in Section 5 of [24], which can be easily adapted to our method.

We start by recalling the local canonical form of $\mathbf{y}(s)$ (cf. (20)):

$$\mathbf{y}(s) = \mathbf{y}(0) + s\mathbf{y}'(0) + \frac{s^2}{2}\mathbf{y}''(0) + \frac{s^3}{6}\mathbf{y}'''(0) + \cdots. \tag{45}$$

Now, for a given step size $h$, we generate $G^1$ Hermite data sampled at $s_0 = 0$ and $s_1 = h$ and apply our interpolation algorithm (see Section 3) to the pairs of adjacent points and tangents. We analyse the existence and behaviour of the MPH interpolant for decreasing step size $h \to 0$. Without loss of generality, we choose $\mathbf{y}(0) = (0, 0, z)^\top$, $\mathbf{T}_0 = (1, 0, 0)^\top$, and $\{\mathbf{N}_0, \mathbf{B}_0\} = \{(0, 1, 0)^\top, (0, 0, 1)^\top\}$, depending on the type of $\mathbf{N}_0$; cf. (18). Moreover, we assume that $\mathbf{y}(s)$ represents a valid MAT (see Section 2.3).

If $\mathbf{N}_0$ is space-like, then this remains valid for $s \in [0, h]$, provided that $h$ is sufficiently small. We remark that $\mathbf{N}_0$ being time-like leads to very similar results with only a few sign changes and that inflections (i.e., the case when $\mathbf{N}_0$ is light-like) have been excluded.

The Taylor expansion of $\mathbf{y}(s)$ is

$$\mathbf{y}(s) = \begin{pmatrix} s - \frac{1}{6}\varkappa_0^2 s^3 - \frac{1}{8}\varkappa_0\varkappa_1 s^4 + \cdots \\ \frac{1}{2}\varkappa_0 s^2 + \frac{1}{6}\varkappa_1 s^3 + \frac{1}{24}(\varkappa_2 + \varkappa_0(\tau_0^2 - \varkappa_0^2))s^4 + \cdots \\ z + \frac{1}{6}\varkappa_0\tau_0 s^3 + \frac{1}{24}(2\varkappa_1\tau_0 + \varkappa_0\tau_0)s^4 + \cdots \end{pmatrix}. \tag{46}$$

Using a suitable computer algebra tool we generate Taylor expansions with respect to $h$ of all quantities occurring in our algorithm. Due to space limitations and the complexity of the expressions, we present only the leading terms of several crucial quantities.

Following the three steps of our algorithm, we start by sampling the data $\mathcal{D}$, i.e., positions and Minkowski unit tangents of $\mathbf{y}(s)$ for $s_0 = 0$ and $s_1 = h$. In Step 1 we find the expansions of the planar data $\overline{\mathcal{D}}$ for PH interpolation; see Section 3.1. This yields that the MAT validity condition (16) reads

$$Q = z\varkappa_0 - 1 < 0. \tag{47}$$

Therefore, from now on we assume that $Q < 0$.

**Table 1**
Numerical results obtained by uniform subdivision in Example 1.

| Segments | Error | Ratio | Segments | Error | Ratio | Segments | Error | Ratio |
|---|---|---|---|---|---|---|---|---|
| 1 | $9.435 \cdot 10^{-2}$ | – | 8 | $8.937 \cdot 10^{-5}$ | 13.08 | 64 | $2.715 \cdot 10^{-8}$ | 15.45 |
| 2 | $1.301 \cdot 10^{-2}$ | 7.25 | 16 | $6.286 \cdot 10^{-6}$ | 14.22 | 128 | $1.727 \cdot 10^{-9}$ | 15.72 |
| 4 | $1.169 \cdot 10^{-3}$ | 11.13 | 32 | $4.195 \cdot 10^{-7}$ | 14.98 | 256 | $1.089 \cdot 10^{-10}$ | 15.86 |

In Step 2 we follow the approach of [35], first discussed in [36], and check that for $\overline{\mathcal{D}}$ there exists a unique simple interpolating PH cubic. Indeed, one can verify that the existence conditions are equivalent to $Q < 0$ provided that $h$ is sufficiently small. For the sake of brevity we omit the details of this purely technical step.

Moving on to Step 3, we verify that the MPH interpolant exists as well. To this end we compute the expansions of the quantities $\sigma_i$ (see (42)) and $\lambda_i$:

$$\sigma_0 = -Qh + \cdots, \qquad \sigma_1 = -Qh + \cdots, \qquad \lambda_0 = h + \cdots, \qquad \lambda_1 = h + \cdots. \tag{48}$$

Thus, under our assumptions, the MPH interpolant exists and preserves the orientation of the end tangent vectors of $\mathcal{D}$ for sufficiently small $h$.

Finally, in order to determine the approximation order of our construction we employ the reparametrisation

$$s(u) = u + \frac{hu(u-1)}{4\varkappa_0 Q}\left[(\varkappa_0 u_0 + \varkappa_1)(1+2Q) + \frac{h(L_0 + L_1 u)}{24\varkappa_0 Q}\right], \tag{49}$$

where $L_0$ and $L_1$ are polynomials in $\varkappa_0, \varkappa_1, \tau_0$ and $Q$ of degree 7 with 15 and 11 terms, respectively. We compare the expansions of the reparametrised MPH interpolant and the given curve $\mathbf{y}$. Since the expansions match up to $h^3$, we conclude that the (geometric) approximation order of our algorithm is equal to 4.

We point out that the approximation order of our method is the same as for the standard interpolation techniques studied in [23,25]. Compared to the $G^1$ scheme, our new algorithm has a very simple existence analysis; cf. Step 3. In fact, an MPH interpolant for $\mathcal{D}$ exists whenever the associated *planar* PH interpolant for $\overline{\mathcal{D}}$ exists and planar scenarios are always much easier to analyse and understand than their spatial analogues. Moreover, our numerous numerical experiments suggest that the approximation order stays 4 at Minkowski inflections and does not drop to 2 as is the case in [23].

Even though we achieve only $G^1$ interpolation compared to the $C^1$ scheme designed in [25] (with MPH curves of degree 5 as well), our new approach is very simple (it does not require the Clifford algebra formalism) and flexible (as discussed in Step 2), and has other advantages as well. Indeed, not only the MAT but also one of the boundary curves can be constructed as polynomial curves. Finally, our method can be easily adapted to rational PH/MPH curves and has potential for generalizations to higher order interpolation schemes.

## 5. Examples

In this section we present numerical results and examples obtained by applying our MPH interpolation scheme.

### 5.1. Example 1

The interpolation algorithm allows us to approximate any space-like analytic curve $\mathbf{c}(t)$ by a quintic MPH spline. Let the parameter domain of $\mathbf{c}(t)$ be $[0, 1]$. Using binary subdivision, we split the interval into $2^n$ segments. For each segment we construct the MPH interpolant. If the error is not sufficiently small, then we continue subdividing. Using an adaptive subdivision could reduce the number of interpolants. Our asymptotic analysis (see Section 4) shows that the error converges to 0 as $\mathcal{O}(16^{-n})$.

We demonstrate the order of convergence with the following example; see Fig. 4. Consider the segment of the $C^\infty$ curve

$$\mathbf{c}(t) = (0.7e^{0.8t}, 1.2 - 0.3\cos t, 0.1 + 0.25t^2)^\top; \quad t \in [0, 1]. \tag{50}$$

We remark that $\mathbf{c}(t)$ satisfies the validity constraints discussed in Section 2.3.

The approximation error (sample-based estimation after the reparametrisation (49)) and its improvement on the first interval span in each step of subdivision are reported in Table 1. The ratios of adjacent errors tend to 16, as predicted from the approximation order.

### 5.2. Example 2

In this example we apply the $G^1$ MPH approximation algorithm to the medial axis transform approximation of a planar region bounded by two curve segments; see Fig. 5. These segments are polynomial quartic arcs $\mathbf{q}(t), \mathbf{r}(t)$ given by their Bézier control points

$$\begin{aligned} &Q_0 = (-1.7, 0.8)^\top, \quad Q_1 = (-1, 0)^\top, \quad Q_2 = (-0.2, -0.5)^\top, \quad Q_3 = (0, 0.3)^\top, \quad Q_4 = (0, 1)^\top, \\ &R_0 = (-2, 0.4)^\top, \quad R_1 = (-1.7, -0.5)^\top, \quad R_2 = (0, -0.8)^\top, \quad R_3 = (1, 0)^\top, \quad R_4 = (1.1, 1)^\top. \end{aligned} \tag{51}$$

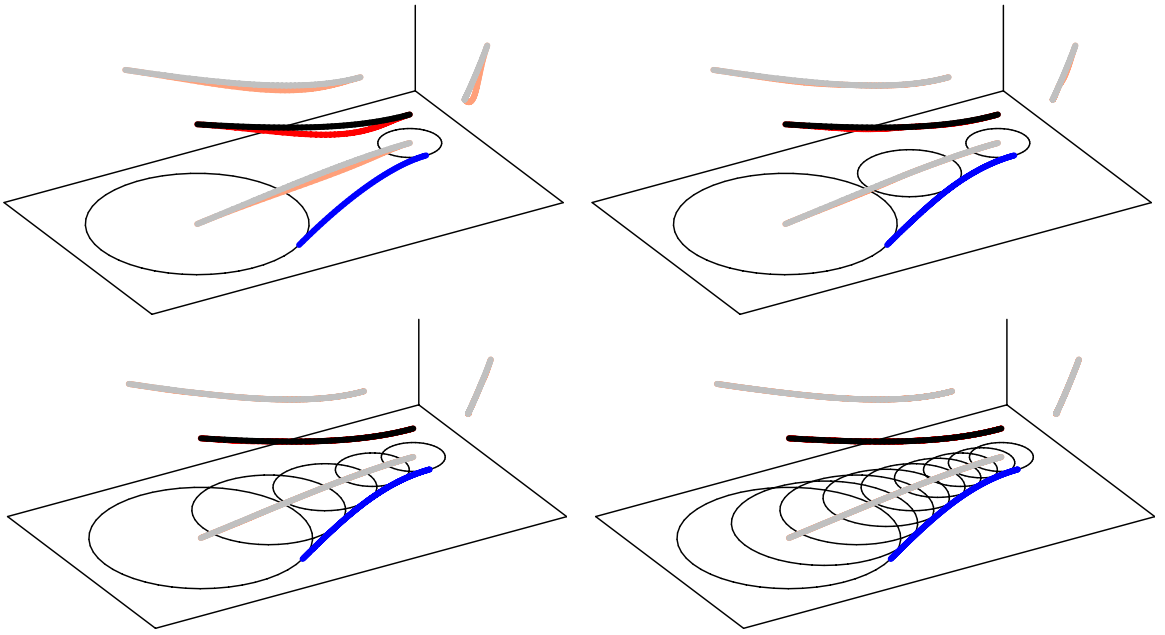

**Fig. 4.** Conversion of an analytic curve (black) into an MPH spline in Example 1. The MPH interpolants are depicted in red, the associated PH spline in blue. (For interpretation of the references to colour in this figure legend, the reader is referred to the web version of this article.)

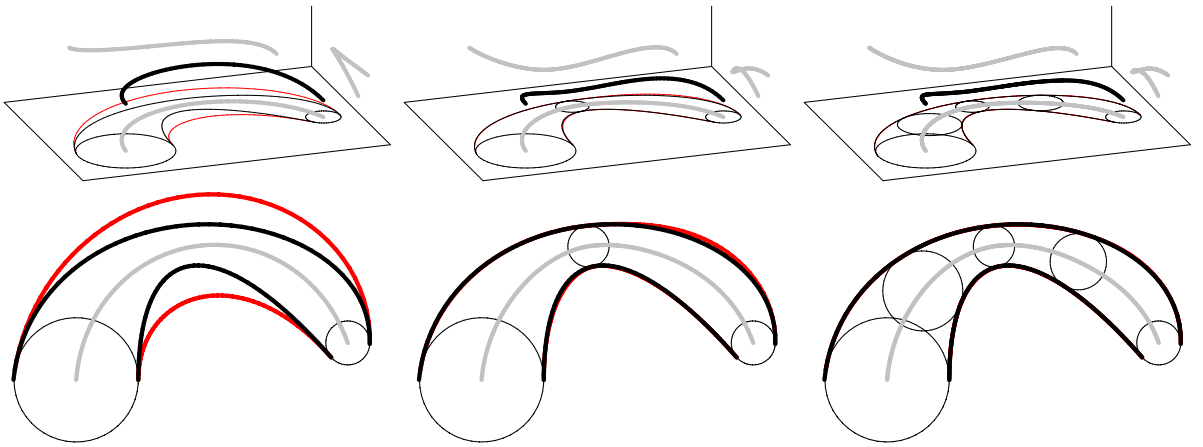

**Fig. 5.** Three steps of subdivision applied to domain boundary approximation in Example 2. Associated domain boundary approximations are depicted in red. Notice that the original boundary (black) is almost indistinguishable from its approximation after only two subdivision steps. (For interpretation of the references to colour in this figure legend, the reader is referred to the web version of this article.)

First, we sample points on $\mathbf{q}(t)$. Then we compute the corresponding points on $\mathbf{r}(t)$ and MAT using a suitable algorithm (e.g. [43]) for finding maximal inscribed discs. These provide us with $G^1$ data which we use in turn for constructing the PH and MPH spline approximation of the original domain's boundary curve $\mathbf{q}(t)$ and MAT, respectively. Finally, using (21) or the envelope formula (8), we compute a rational PH spline approximation of the domain boundary curve $\mathbf{r}(t)$. Also, we can start with sampling points on $\mathbf{r}(t)$. The method then gives almost indistinguishable results after only one step of subdivision.

We remark that this scheme has approximation order 4 as well. This fact follows from the asymptotic analysis presented in Section 4 and the result (47) of Kosinka and Jüttler [24].

### 5.3. Example 3

In this example we demonstrate the advantage of the MAT representation of a planar domain $\Omega$ on the trimming process of the inner offsets of $\Omega$. Consider again the domain in Example 2 enclosed by two quartic arcs $\mathbf{q}(t)$, $\mathbf{r}(t)$. Several (untrimmed) inner offsets of this domain are depicted in Fig. 6, left. Once we have a suitable approximation of the MAT of $\Omega$ at hand (cf. Example 2), we simply remove the parts of the MAT (and the associated offset curves) for which the corresponding

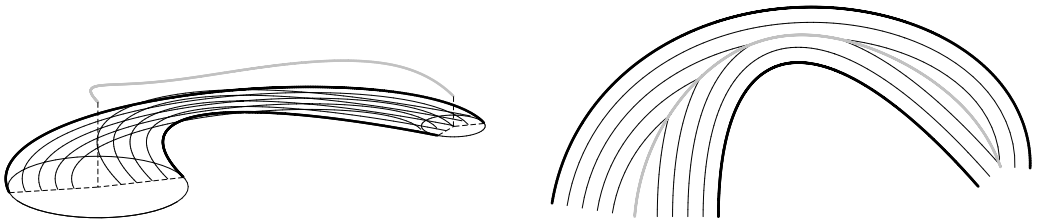

**Fig. 6.** Untrimmed inner offsets (left) and inner offsets after trimming (right). The MA and MAT approximations are depicted in grey. (For interpretation of the references to colour in this figure legend, the reader is referred to the web version of this article.)

MAT radius is less than the offset distance; see Fig. 6, right. For this particular example, three subdivision steps were used (i.e., one more than in Example 2, Fig. 5).

## 6. Conclusion

In the present paper we continued the discussion of the interplay between spatial MPH curves and associated planar PH curves started in [21] from the point of view of Hermite interpolation schemes. We introduced a novel approach for interpolating a spatial space-like curve considered as the medial axis transform of a planar domain. In addition, the MAT validity conditions with respect to given interpolation data were thoroughly studied.

The main advantage of the scheme presented is its simplicity. An arbitrary (and at any time replaceable) algorithm for interpolation using planar PH curves is used after some simple additional computations also for interpolation using spatial MPH curves. The scheme presented provides a nice geometric insight, and unlike available MPH schemes (e.g. $C^1$) does not require the complicated Clifford algebra machinery and uses already well-known and established results for planar PH curves. The approximation order of the algorithm designed is 4, including inflection points. This is an improvement compared to other known $G^1$ techniques working directly in the Minkowski space, where the approximation order drops to 2 at inflections. The technique presented can be used 'as is' also for computing polynomial/rational approximations of real-domain boundaries and all their (trimmed) offsets. Furthermore, this algorithm has another useful advantage—not only the MAT but also one of the boundary curves can be constructed as a polynomial curve.

In our future work, we would like to focus on higher order relations. Promising results on connections between the Minkowski curvature of an MPH curve and the curvatures of its associated planar PH curves (cf. [21]) give a good chance to design an analogous (and also simple) $G^2$ Hermite interpolation scheme. Finally, it is certainly a challenge to generalize this scheme to MOS surfaces constructed from associated PN surfaces in the spirit of [44].

## Acknowledgements

The work on this paper was supported by the Research Plan MSM 4977751301. We thank all referees for their comments, which helped us to improve the paper.

## References

[1] W. Lü, H. Pottmann, Rational parameterization of quadrics and their offsets, Computing 57 (1996) 135–147.
[2] E. Arrondo, J. Sendra, J.R. Sendra, Parametric generalized offsets to hypersurfaces, Journal of Symbolic Computation 23 (1997) 267–285.
[3] E. Arrondo, J. Sendra, J.R. Sendra, Genus formula for generalized offset curves, Journal of Pure and Applied Algebra 136 (1999) 199–209.
[4] T. Maekawa, An overview of offset curves and surfaces, Computer-Aided Design 31 (1999) 165–173.
[5] J.R. Sendra, J. Sendra, Algebraic analysis of offsets to hypersurfaces, Mathematische Zeitschrift 237 (2000) 697–719.
[6] M. Lávička, B. Bastl, Rational hypersurfaces with rational convolutions, Computer Aided Geometric Design 24 (7) (2007) 410–426.
[7] J. Vršek, M. Lávička, On convolution of algebraic curves, Journal of Symbolic Computation 45 (6) (2010) 657–676.
[8] R. Farouki, T. Sakkalis, Pythagorean hodographs, IBM Journal of Research and Development 34 (5) (1990) 736–752.
[9] R. Farouki, T. Sakkalis, Pythagorean-hodograph space curves, Advances in Computational Mathematics 2 (1994) 41–66.
[10] R. Farouki, C. Manni, A. Sestini, Spatial $C^2$ PH quintic splines, in: T. Lyche, M. Mazure, L. Schumaker (Eds.), Curve and Surface Design: St. Malo 2002, Nashboro Press, 2003, pp. 147–156.
[11] Z. Šír, B. Jüttler, Euclidean and Minkowski Pythagorean hodograph curves over planar cubics, Computer Aided Geometric Design 22 (8) (2005) 753–770.
[12] R. Farouki, T. Sakkalis, Rational space curves are not unit speed, Computer Aided Geometric Design 24 (2007) 238–240.
[13] Z. Šír, B. Jüttler, $C^2$ Hermite interpolation by Pythagorean hodograph space curves, Mathematics of Computation 76 (2007) 1373–1391.
[14] H. Pottmann, Rational curves and surfaces with rational offsets, Computer Aided Geometric Design 12 (2) (1995) 175–192.
[15] R.T. Farouki, H. Pottmann, Polynomial and rational Pythagorean-hodograph curves reconciled, in: Proceedings of the 6th IMA Conference on the Mathematics of Surfaces, Clarendon Press, New York, NY, USA, 1996, pp. 355–378.
[16] B. Bastl, B. Jüttler, J. Kosinka, M. Lávička, Computing exact rational offsets of quadratic triangular Bézier surface patches, Computer-Aided Design 40 (2008) 197–209.
[17] M. Lávička, B. Bastl, PN surfaces and their convolutions with rational surfaces, Computer Aided Geometric Design 25 (2008) 763–774.
[18] R. Farouki, Pythagorean-Hodograph Curves: Algebra and Geometry Inseparable, Springer, 2008.
[19] H.I. Choi, C.Y. Han, H.P. Moon, K.H. Roh, N.-S. Wee, Medial axis transform and offset curves by Minkowski Pythagorean hodograph curves, Computer-Aided Design 31 (1) (1999) 59–72.
[20] H. Moon, Minkowski Pythagorean hodographs, Computer Aided Geometric Design 16 (1999) 739–753.
[21] J. Kosinka, M. Lávička, On rational Minkowski Pythagorean hodograph curves, Computer Aided Geometric Design 27 (7) (2010) 514–524.

[22] H. Choi, D. Lee, H. Moon, Clifford algebra, spin representation and rational parameterization of curves and surfaces, Advances in Computational Mathematics 17 (2002) 5–48.
[23] J. Kosinka, B. Jüttler, Cubic helices in Minkowski space, Sitzungsberichte. Oesterreichische Akademie der Wissenschaften, Mathematisch-Naturwissenschaftliche Klasse, Abteilung II (Mathematik, Astronomie, Physik, Meteorologie und Technik) 215 (2006) 13–35.
[24] J. Kosinka, B. Jüttler, $G^1$ Hermite interpolation by Minkowski Pythagorean hodograph cubics, Computer Aided Geometric Design 23 (2006) 401–418.
[25] J. Kosinka, B. Jüttler, $C^1$ Hermite interpolation by Pythagorean hodograph quintics in Minkowski space, Advances in Computational Mathematics 30 (2009) 123–140.
[26] J. Kosinka, Z. Šír, $C^2$ Hermite interpolation by Minkowski Pythagorean hodograph curves and medial axis transform approximation, Computer Aided Geometric Design 27 (8) (2010) 631–643.
[27] Z. Šír, J. Kosinka, Low degree Euclidean and Minkowski Pythagorean hodograph curves, in: M. Dæhlen, M. Floater, T. Lyche, J.-L. Merrien, K. Mørken, L. Schumaker (Eds.), Mathematical Methods for Curves and Surfaces, in: Lecture Notes in Computer Science, vol. 5862, Springer, Berlin, Heidelberg, 2010, pp. 394–418.
[28] H. Choi, S. Choi, H. Moon, Mathematical theory of medial axis transform, Pacific Journal of Mathematics 181 (1997) 57–88.
[29] C.M. Hoffmann, P.J. Vermeer, Validity determination for MAT surface representation, in: Proceedings of the 6th IMA Conference on the Mathematics of Surfaces, Clarendon Press, New York, NY, USA, 1996, pp. 249–265.
[30] R.C. Teixeira, Medial axes and mean curvature motion I: regular points, Journal of Visual Communication and Image Representation 13 (1–2) (2002) 135–155.
[31] P. Yushkevich, P.T. Fletcher, S. Joshi, A. Thall, S.M. Pizer, Continuous medial representations for geometric object modeling in 2D and 3D, Image and Vision Computing 21 (1) (2003) 17–27.
[32] R. Krasauskas, C. Mäurer, Studying cyclides with Laguerre geometry, Computer Aided Geometric Design 17 (2) (2000) 101–126.
[33] M. Peternell, H. Pottmann, A Laguerre geometric approach to rational offsets, Computer Aided Geometric Design 15 (1998) 223–249.
[34] H. Pottmann, M. Peternell, Applications of Laguerre geometry in CAGD, Computer Aided Geometric Design 15 (1998) 165–186.
[35] M. Byrtus, B. Bastl, $G^1$ Hermite interpolation by PH cubics revisited, Computer Aided Geometric Design 27 (8) (2010) 622–630.
[36] D.S. Meek, D.J. Walton, Geometric Hermite interpolation with Tschirnhausen cubics, Journal of Computational and Applied Mathematics 81 (2) (1997) 299–309.
[37] G. Jaklič, J. Kozak, M. Krajnc, V. Vitrih, E. Žagar, Geometric Lagrange interpolation by planar cubic Pythagorean-hodograph curves, Computer Aided Geometric Design 25 (9) (2008) 720–728.
[38] E. Černohorská, Z. Šír, Support function of Pythagorean hodograph cubics and $G^1$ Hermite interpolation, in: B. Mourrain, S. Schaefer, G. Xu (Eds.), Advances in Geometric Modeling and Processing, in: Lecture Notes in Computer Science, vol. 6130, Springer, Berlin, Heidelberg, 2010, pp. 29–42.
[39] D.S. Meek, D.J. Walton, Approximating smooth planar curves by arc splines, Journal of Computational and Applied Mathematics 59 (2) (1995) 221–231.
[40] Z. Šír, R. Feichtinger, B. Jüttler, Approximating curves and their offsets using biarcs and Pythagorean hodograph quintics, Computer-Aided Design 38 (2006) 608–618.
[41] X. Yang, Z.C. Chen, A practicable approach to $G^1$ biarc approximations for making accurate, smooth and non-gouged profile features in CNC contouring, Computer-Aided Design 38 (11) (2006) 1205–1213.
[42] Z. Šír, B. Bastl, M. Lávička, Hermite interpolation by hypocycloids and epicycloids with rational offsets, Computer Aided Geometric Design 27 (2010) 405–417.
[43] O. Aichholzer, F. Aurenhammer, T. Hackl, B. Jüttler, M. Oberneder, Z. Šír, Computational and structural advantages of circular boundary representation, in: F. Dehne, J.-R. Sack, N. Zeh (Eds.), Algorithms and Data Structures, in: Lecture Notes in Computer Science, vol. 4619, Springer, Berlin, Heidelberg, 2007, pp. 374–385.
[44] M. Peternell, Rational two-parameter families of spheres and rational offset surfaces, Journal of Symbolic Computation 45 (1) (2010) 1–18.